

Drying of a model soil

P. Faure and P. Coussot

Laboratoire Navier, Université Paris-Est, Champs sur Marne, France

(Received 30 April 2010; published 2 September 2010)

Drying experiments have been carried out with model soils made of different pastes filling granular packings. A detailed information concerning the time evolution of the water saturation distribution inside the sample was obtained from magnetic resonance imaging measurements. This study makes it possible to understand the physical origin of the drying characteristics of these materials. The drying curves exhibit a constant-rate period (CRP) and a falling-rate period (FRP) but the relative durations of these periods depend on the paste structure. With a kaolin suspension the CRP lasts down to very low water densities and is associated with a homogeneous drying of the paste throughout the sample. With a bentonite suspension the CRP is shorter and the drying in the FRP results from a complex process involving fractures progressing downward through the pasty matrix. With a gel the CRP period is even shorter and the drying in the FRP results from the progression of a dry front through the packing as a result of the shrinkage of the gel matrix. This provides an overview of the main possible processes at work when drying a soil as a function of its components along with some practical means for slowing down drying from soils.

DOI: [10.1103/PhysRevE.82.036303](https://doi.org/10.1103/PhysRevE.82.036303)

PACS number(s): 47.56.+r, 92.40.Je, 47.57.J-

I. INTRODUCTION

Drying plays an important role in the various industrial processes that at some steps involve wet materials. It is the case in food industry, mineral industry, civil engineering, etc. [1]. Soil drying also plays a critical role in agriculture: an inadequate water supply may limit crop production, and soil water evaporation is a primary factor contributing to limit water supply. In order to predict its characteristics or to devise methods to control drying it is useful to fully understand the physics of soil drying.

Concerning the evaporation from soils the classical view is a two stage process [2,3]. In the first, constant-rate, stage [constant-rate period (CRP)] the drying rate is approximately constant and it is considered that this results from a transport of the liquid to the surface of the sample driven by capillary effects at a rate controlled by atmospheric conditions. In the second, falling-rate, stage [falling-rate period (FRP)] the drying rate progressively decreases down to low values. A third stage is also sometimes considered [4], during which the drying rate remains at an almost constant low value and might be controlled by adsorptive forces acting over molecular distances at the solid-liquid interfaces. In addition shrinkage and fracture may be sometimes observed [5].

In some cases a major part of the water evaporates during the second stage. However, the processes at work are somewhat debated. It has been suggested that this can be due to the increase of resistance to water flow within the sample (as the liquid film thickness decreases) [6] or to the decrease of the evaporation rate as the top layers of the sample surface dry out [7]. Various models have attempted to describe the decrease in water content during this stage using material parameters [3]. In particular, Ritchie [8] provided a model based on the diffusivity theory and relying on a single material parameter. Although this model features some generic physical approach it does not take into account the various possible structures of soils and their impact on the process. Indeed, it appears that soils exhibit macroscopic characteris-

tics varying from one material to another as a function of their components, but no physical approach was carried out to account for the physical processes at work while drying and how it may change depending on the material structure.

In contrast in recent years a strong effort was made to understand the physical process at work during the drying of model materials mainly made of a simple solid porous material (usually a bead packing) and a pure liquid. In that case a similar three-stage process is also observed and was explained as follows [9]:

(i) The initial stage, CRP, corresponds to an evaporation process sufficiently slow as compared to the ability of the liquid to move to the sample surface under the action of capillary effects; thus, the drying rate is controlled by ambient conditions (air flow, temperature, and hygrometry).

(ii) The second stage, FRP, results from an evaporation demand higher than the ability of the liquid to move toward the surface as a result of capillary forces; thus, the drying rate is controlled by a balance between capillary forces and viscous flow. During this period a thin dry region forms around the sample surface.

(iii) In the third stage, during which there is no possible balance between capillary effects and viscous flow, drying essentially results in the penetration of a dry front from the free surface through the sample; then, the rate of drying is mainly controlled by diffusion effects through the dry region.

Basic scaling arguments [10] and more sophisticated descriptions [11] were provided for these different regimes. Direct visualizations from dye transport and deposition [12], neutron radiography [13], gamma-ray densimetry [14], x-ray tomography [15], magnetic resonance imaging (MRI) [16], or confocal microscopy [17], with samples of controlled wetting characteristics or controlled pore size, provided an insight in different local characteristics and finally confirmed the different physical arguments of the above global scheme. In addition various studies with simplified porous structures [18–22] provided valuable information concerning the exact physical processes occurring at a local scale such as the in-

fluence of film shapes, pore shapes, and wetting characteristics.

For soils, although the basic explanations for the first two drying stages make sense, there is no clear-cut evidence because it is much more difficult to get measurements of properties inside the sample. Actually contrary to model bead packings a soil contains particles whose size ranges from large (for silt, sand, pebbles, etc.) to very small (for clay) with additional organic matter of various sizes and properties. It is nevertheless possible to make a useful distinction between these different elements. Beyond some critical size the particles do not develop any interaction at distance and the Brownian motion is negligible. If these particles were alone in water the drying characteristics of the sample would be similar to those above described because the water can rather easily flow through a packing of such particles. Below this particle size we are in the colloidal range; the particles develop strong interactions that vary significantly with their separating distance. As a consequence the energy needed to extract water from such a mixture is larger because this extraction implies a decrease of the distance between the particles, which usually leads to increased colloidal forces. These colloidal particles generally form with water, which we can call a paste, i.e., typically a yield stress fluid [23]. In practice it is not so easy to determine the precise value of this critical size. Moreover, the impact of the colloidal nature of the particle on the drying characteristics under ambient conditions looks unimportant likely because capillary effects can still govern the processes. Anyway, this naturally suggests that a basic model soil should be made of coarse particles immersed in a paste (colloids+water). The present work relies on this assumption which might be the first step toward a more accurate description. In this respect we can expect processes more complex than with the liquid in bead packings. Indeed, the water may move either out of the paste or with the paste through the granular network up to the sample surface.

Now, in order to understand these physical processes we will focus on a model soil made of a paste, i.e., a mixture of water with a colloidal phase forming a non-Newtonian fluid with a yield stress, inside the pores of a granular packing. This relatively simple material may be seen as exhibiting some of the basic trends of the structure of a wide range of real soils: a granular structure allowing supporting heavy vertical loads and an interstitial colloidal phase mixed with the liquid. Note that the present approach does not encompass materials for which the granular phase concentration is smaller than the maximum packing fraction. Indeed, in that case the interstitial paste will very likely govern the behavior of the sample so that macroscopic shrinkage and fractures may occur and play a critical role on the drying characteristics.

Although the question of drying of a paste within a granular packing is the natural next step toward a fundamental understanding of soil drying, it is quite open. A paste is indeed a yield stress fluid which can flow at a slow flow rate only if a stress larger than a finite value is not applied. Such a behavior might tend to prevent the paste from moving toward the free surface of the sample and thus impair capillary transport. Under such conditions one could expect the form-

ing of a crust in the top layers, i.e., a region of paste much more concentrated than the rest of the paste. However, with appropriate paste components one could also expect some capillary effects through the paste itself.

We carried out tests with similar bead packings and different interstitial pastes of various internal structures. We obtained macroscopic facts on the drying characteristics from mass measurements and local information from magnetic-resonance imaging measurements. We could thus identify thoroughly the drying regimes for such materials and in particular show that very different behavior types can be obtained depending on the specific structure of the paste. We start by presenting the materials and procedures (Sec. II); then, we proceed with a preliminary review of the characteristics of the main possible drying regimes which may be expected in this context (Sec. III). At last we present the data and an analysis and discussion of the results (Sec. IV).

II. MATERIALS AND PROCEDURES

A. Material preparation

As materials we used mixtures of glass beads and different types of pastes. As pastes we used a kaolin-water suspension at a solid volume fraction of 21% except when mentioned. The kaolin was a natural clay with a density of about 2650 kg m^{-3} which has been purified (China clay, *Speswhite*, Great Britain). It is made of small platelet particles (with a typical largest size of $1 \text{ }\mu\text{m}$ and an aspect ratio about 10) with almost no colloidal interactions. We also used a Na-bentonite-water suspension (solid volume fraction: 4%) prepared from industrial grade bentonite (*Société française des bentonites et dérivés*, France) thoroughly mixed with distilled water, then left at rest several weeks to allow for hydration and dispersion of the clay particles. The bentonite is a natural swelling clay with a density of about 2650 kg m^{-3} which has been purified. It is made of slightly flexible large aspect ratio smectite particles (of maximum length on the order of $1 \text{ }\mu\text{m}$ and an aspect ratio on the order of 100) inside which water tends to penetrate but which can aggregate via edge-to-face links thus forming a solid structure at rest so that the suspension may be seen as a colloidal gel. Finally, we used a hair gel (*Vivelle Dop*, France). Such a hair gel is mainly made of Carbopol (reticulated polyacrylic acid resins) in water. The structure of a Carbopol suspension is liable to depend on the exact characteristics of the material used, but in general its molecules arrange in roughly spherical blobs which tend to swell in water (see, for example, [24]). As a consequence, beyond a critical concentration the blobs are squeezed against each other. Piau [25] described the structure of a Carbopol gel as a “polydisperse glass made of swollen hydrophylic elastic sponges.”

The glass beads (with a diameter of $300 \pm 50 \text{ }\mu\text{m}$ except when mentioned) were then added to one of these pastes so as to get a volume concentration of the beads (total bead volume/sample volume) of 62% in the final mixture and gently mixed until obtaining apparently homogeneous mixtures. The resulting granular mixtures were then put in cylindrical vessels with diameter of 34 mm, and we used vessels of different heights and filled them up to about 1 mm from the

top. The initial sample height is noted L_0 . Note that air volumes are easily trapped when mixing the paste and the beads. In order to remove most bubbles remaining within the mixture the vessel was manually tapped for few minutes making the bubbles slowly move upward. There nevertheless remained a slight fraction of bubbles (on the order of 1%) trapped in the material.

Under such conditions we get granular packings in which the voids are filled with a paste, the elements of which are much smaller than the grain size, and which, in fact, initially forms a continuous matrix in which the grains may be considered as embedded. However, since the grain fraction is close to the maximum disordered packing fraction (say around 64%) [23], a significant further compaction of grains during drying is not possible.

The samples were then left drying in a quiet room at ambient temperatures. We thus aimed at reproducing somewhat uncontrolled ordinary conditions of drying of real soils for which the wind direction and strength may significantly vary in time. In our case the temperature fluctuated in the range of 19–22 °C and the hygrometry between 40% and 60%. However, the temperature and hygrometry were on average constant over our long periods of tests (a typical test lasts several weeks). Moreover, by repeating the tests we were able to show that these fluctuations have a negligible impact on the results presented here. We either measured the sample mass in time with a scale or measured the vertical apparent water saturation profile by NMR (see the procedure below). From the first type of measurement we deduce the total saturation, Φ , defined as the ratio of the total current water content to the initial one. From the NMR profiles which basically provide estimates of the local water content we estimate the local saturation $\phi(x)$, i.e., the total saturation within a thin layer of sample at a distance x . Obviously, if the corresponding measures are consistent we expect that $\Phi = (1/L_0) \int_0^{L_0} \phi dx$.

B. Paste characteristics

Our different pasty materials are basically yield stress fluids; i.e., they behave as viscoelastic solids below a critical stress and flow like liquids for a stress larger than this critical value which is referred to as the yield stress, noted τ_c . The kaolin suspensions [26] and the gel [27] are relatively simple yield stress fluids with no significant time-dependent properties (thixotropy). Their steady-state behavior in the liquid regime is well represented by a Herschel-Bulkley model; i.e., the stress is the sum of the yield value (τ_c) plus a term proportional to a power law of the shear rate. The rheological behavior of the bentonite suspensions is significantly more complex: the material ages at rest, so that its apparent yield stress increases with the time of rest, and rejuvenates during flow, so that its apparent viscosity decreases with the duration of flow [28].

Since this is a process which might play some role in the drying of our granular packings it is useful to analyze how the pastes alone dry. The kaolin suspensions we used dry at a constant rate, associated with a homogeneous shrinkage, during a relatively long time (typically down to a saturation of

about 10%); then, they start to fracture. Such a behavior is typical of the drying of clay materials [5,29]. For the bentonite suspension we have a much shorter constant-rate period before fracturing. For the gel we have a short homogeneous shrinking period followed by a phase during which the gel fractures and go on shrinking, a typical process in gel drying [30]. These trends result from the structures of the pastes: the kaolin suspension contains solid clay particles able to approach each other without significant colloidal interactions so that water evaporation can easily shrink the sample homogeneously; in the bentonite the particles develop strong attractive colloidal interactions so that extracting water can hardly shrink the sample homogeneously and rather leads to fractures. As for the gel, during drying it tends to displace on the solid surface of the container, so that the final dry deposit may cover an area significantly smaller than the initial layer area. Once again this is the difficulty for shrinking homogeneously the elements within the gel which leads to such processes.

Anyway it is difficult to obtain relevant quantitative characteristics of paste drying since the free surface of the sample either moves downward in the container (if the material shrinks) or becomes much more complex (if the material fractures) during drying. This implies the *surface of evaporation*, i.e., the surface of the sample fully exposed to the air stream is not constant: it strongly varies in time as a function of the deformation, fracture, or shrinkage of the material. In contrast, with the granular packing filled with pastes, because of the incompressibility of the bead packing the surface of evaporation is approximately constant. This is a fundamental aspect which, in particular, suggests that we have here an appropriate way for characterizing the drying behavior of pastes under given conditions along the process.

C. NMR

1. Equipment and procedures

NMR studies were performed on a vertical imaging spectrometer DBX 24/80 Bruker operating at 0.5 T (20 MHz proton) and equipped with a birdcage radio frequency coil of 20 cm inner diameter. Such low magnetic field is suited for porous material studies: it indeed maintains the susceptibility induced field inhomogeneities inside the sample at a moderate level while enhancing surface relaxation effects of water molecules on paramagnetic centers [31], which is a key phenomenon for relaxation study of porous systems. The main advantage of working with such wide bore facility is to be able to study centimetric samples, which are real bulk materials with negligible edge effects. The main drawback of working with big size spectrometer is the long delay needed to perform rf pulses. Here hard $\pi/2$ and π pulse durations were 110 and 220 μ s, respectively.

The NMR signal recorded is essentially sensitive to the excitation of the spins of the water hydrogen protons. The initial (for saturated samples) T_1 relaxation times were 40 ms for the kaolin suspension, 41 ms for the bentonite suspension, and 380 ms for the gel. As a consequence the lifetime of the water NMR signal in these pastes is sufficiently long for conventional MRI methods to be used. We measured the

distribution (profile) of apparent water density along the sample axis with the help of a one-dimensional double spin-echo sequence (two first echoes of the so-called Carr-Purcell-Meiboom-Gill sequence [32]) with magnetic field pulse gradient along the central axis of the sample. The signal thus measured corresponds to the total NMR signal in a thin (cross-sectional) layer situated at a given position along sample axis. We imposed the following relaxation delays (T_R)—250 ms for kaolin and bentonite and 4 s for the gel—and the following number of repetition of the sequence—2048 for kaolin and bentonite and 128 for the gel—which led to typical test duration of 10 min. The echo time T_E is 7 ms. In some cases for low saturations we increased the repetition number. We also measured the apparent water density distribution (images) in a two-dimensional (2D) layer with thickness of 5 mm along the central axis. In that aim we used the more classical spin-echo sequence (with spin echo and three magnetic field pulse gradients in the three space directions). The image dimensions were 13×7 cm with a matrix of 128×64 and the acquisition duration was around 2 min ($T_R=250$ ms and 2 s for kaolin and bentonite, respectively, and number of repetition of the sequence: eight for kaolin and bentonite and one for the gel).

2. Data correction

The initial (i.e., before drying) NMR density profiles are somewhat uneven [see Fig. 1(a)], whereas we would expect (horizontal) straight lines since the paste concentration is *a priori* independent of the depth and the water concentration in the paste is homogeneous. This effect may nevertheless be due to some heterogeneities of the porous distribution of the grain packing at the scale of the thin layers associated with each data point, leading to heterogeneities of the apparent water density; such an effect is at least likely the origin of the small wavelength variations. There may also be some slight spatial variations of the magnetic field; such an effect is likely at the origin of the large wavelength variations. Since during the tests the effects of magnetic field variations should induce constant relative variations of the NMR signal we can remove their impact by dividing each density profile obtained after some drying by the profile measured at the initial time. This procedure may also somewhat remove the impact of local heterogeneities of the porous structure. At last, as we divide the apparent current local water density by the initial (maximum) value we directly obtain profiles of the apparent signal saturation as measured by NMR: ϕ_{NMR} [see Fig. 1(b)]. Moreover the NMR signal is affected by a noise, the maximum level of which depends on each material. We removed the data points which were below this level and focused on data corresponding to NMR signal above this level.

For given solid-liquid interaction the signal intensity is simply proportional to the water density, but as soon as the water content varies within a porous structure the relaxation time varies; it, in particular, decreases with the pore size and thus decreases as the local water fraction decreases. Thus, the measured signal intensity depends not only on the water density but also on the local structure and the corresponding relaxation process. In the NMR sequence used

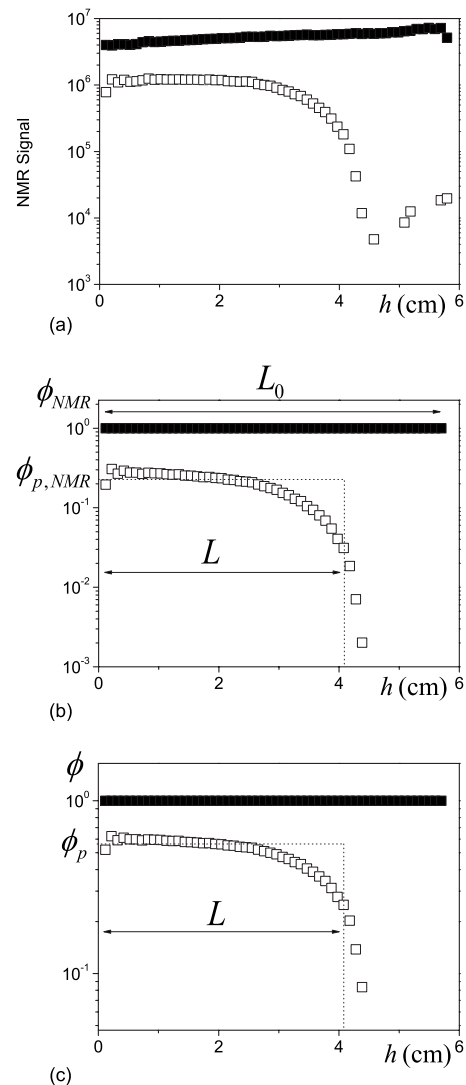


FIG. 1. Apparent water density or saturation profiles in the bentonite sample in Fig. 11(a) at the initial time (filled squares) and after 21 days of drying (open squares): (a) apparent density as measured by NMR; (b) apparent saturation after correction for the sample or magnetic field heterogeneities; and (c) after additional correction for relaxation effects.

the signal is affected by the relaxation effects by a factor $[1 - \exp(-T_R/T_1)] \exp(-T_E/T_2)$ (in which T_2 is the second NMR relaxation time). This factor is negligibly different from 1 at the beginning of the experiment since $T_R/T_1 > 5$ and $T_E/T_2 < 5$. However, for example, for a bentonite sample, T_1 decreased by a factor larger than 2 when the saturation varied from 1 to 0.25 as a result of drying. This implies that the decrease of the relaxation times of the samples has an impact on our measurements. Rather than trying to model these complex phenomena we followed the simple straightforward procedure below for a relevant analysis of NMR data in terms of effective local water saturation.

For all the materials the apparent density profiles obtained from NMR measurements are always approximately composed of a plateau starting from the sample bottom and a relatively rapid decrease toward lower values around some depth. This implies that the integral of the NMR signal over

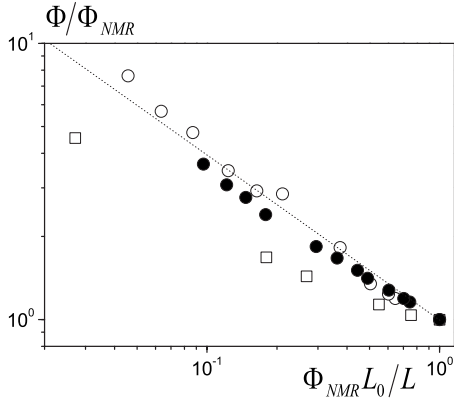


FIG. 2. Ratio of the effective water saturation (obtained from sample weighting) to the NMR signal saturation as a function of the NMR signal saturation for the kaolin (squares) and bentonite samples in Fig. 11(a) (open circles) and Fig. 11(b) (filled circles). The inclined dotted line corresponds to a power-law model with a power of $-2/3$.

the sample thickness is essentially proportional to the plateau level and to its thickness [see Fig. 1(b)]. It is natural to assume that the NMR signal is a simple increasing function of the effective water density tending to zero when the water density tends to zero. As a consequence we expect the same trend for the effective water density profile: as a first approximation it should be essentially a plateau from the bottom up to a depth identical to the critical depth for the NMR signal. Thus, during drying the level of the plateaus for the effective water density profile and for the NMR signal intensity may vary in a different way but the length of the plateaus, $L(t)$, varies in a similar way. More precisely we may write the total water saturation (over the sample height) as $\Phi(t) \approx L(t)\phi_p(t)/L_0$ and the integral of the NMR signal saturation over the sample height as $\Phi_{NMR}(t) \approx L(t)\phi_{p,NMR}(t)/L_0$, in which $\phi_p(t)$ and $\phi_{p,NMR}(t)$ are the plateau levels at time t for the profiles of the water saturation and the NMR signal saturation, respectively. As a consequence the relationship between a given NMR signal intensity and the water density may be found from the ratio of $\phi_{p,NMR}(t)$ to $\phi_p(t)$, which is equal to $\Phi_{NMR}(t)/\Phi(t)$, in which $\Phi(t)$ is deduced from mass measurements and $\Phi_{NMR}(t)$ by integration of the NMR signal over the sample height. We plotted $\Phi/\Phi_{NMR} = \phi_p/\phi_{p,NMR}$ as a function of $\Phi_{NMR}L_0/L \approx \phi_{p,NMR}$ for the kaolin and bentonite samples at different times (see Fig. 2). For both samples the NMR saturation significantly increases with the water saturation: for example, for the bentonite sample we approximately have $\phi_p \propto \phi_{p,NMR}^{1/3}$. We corrected the NMR density profiles according to the variations observed in Fig. 2; this, for example, gives the profile of Fig. 1(c). This provides still somewhat approximate density profiles since the NMR profiles generally do not correspond exactly to a plateau of given length, but they represent qualitatively very well the effective density distribution in time. For the gel the plateau level remains close to the initial saturation, which implies that this is also true for the water saturation. As a consequence the water saturations estimated from the mass measurements and from the NMR signal are very close to each other (see Fig. 14). Remark that

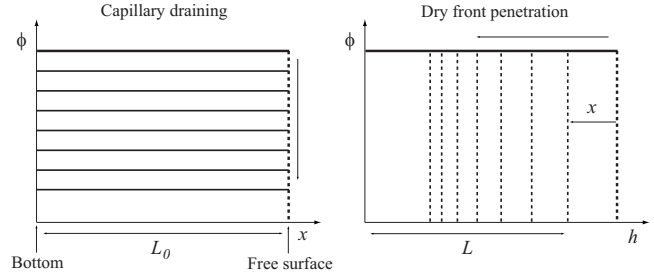


FIG. 3. Theoretical saturation profiles in the sample for case (a) (left) and case (b) (right) as described in the text.

the local NMR measurements for local saturation lower than 1 may be affected by relaxation effects but our approach does not make it possible to quantify this effect with this material. Thus, we did not make any correction to the NMR profiles for the gel.

III. THEORETICAL CONSIDERATIONS

Here, we review the basic processes by which such materials may dry. We can distinguish two different processes. In the first process the water is embedded in a solid matrix made of the beads plus the paste elements and through which it moves. In the second process the water is embedded in a paste through which it can hardly move. In each case we can estimate the drying characteristics in some specific situations.

A. Water transport through fixed paste-bead mixture

In that case there are two “asymptotic” simple ways by which the material can dry in the absence of thermal effects. As for a simple granular packing with pure water one can consider a strictly *capillary process* [case (a)] in which the water mainly evaporates along the free surface and is moved toward this surface by capillary effects through the paste and the granular packing. Conversely, we can consider a situation [case (b)] for which the water is unable to be drained toward the free surface of the sample, so that the liquid region closest to this surface progressively evaporates: then, a dry front progresses inward the bead pack (see Fig. 3).

In case (a) the rate of drying is constant since, due to the multiple small water patches dispersed around this region, the vapor density remains at its maximum value just above the free surface of the sample [10], so that we have $dm/dt = Cst$, in which m is the mass of water. Moreover, these patches are connected to a liquid network throughout the sample, so that the mass loss in time induces a homogeneous decrease of the water saturation in the sample, i.e., $L(t) = L_0$, which implies $m \propto L_0\Phi = \phi L_0$ (see Fig. 3). For a free surface of given area and shape we deduce $L_0 d\phi/dt = -k$, where k is a constant. This equation may be integrated to give

$$\phi = \phi_0 - k \frac{t}{L_0}. \tag{1}$$

Thus, in that case we have a linear variation of the saturation in time and an independence of the saturation on the sample

size when the time is scaled by the sample height.

In case (b) the rate of drying is proportional to the gradient of vapor density, which actually is uniform, between the wet surface within the sample and the free surface of the sample [16], so that $dm/dt \propto \Delta n/x$, where Δn is the difference between the maximum vapor density and the vapor density in the air above the sample and x is the distance between the wet front and the free surface of the sample. Since for a given cross section of the sample we also have $m \propto (L_0 - x)$, we can integrate the above equation and get

$$\phi = \phi_0 - k^* \sqrt{\frac{t}{L_0^2}}, \quad (2)$$

in which ϕ_0 is the (uniform) saturation at the initial time when the drying front starts to recede within the sample.

With pure water in a granular packing case (a) generally occurs over a long period and then case (b) takes place when the saturation is so low and liquid films are so thin (or there is no more continuous liquid network) that capillary effects are unable to suck liquid toward the free surface of the sample. This scheme is the usual straightforward explanation for the CRP and the FRP.

B. Flow of paste through bead skeleton

Here we assume that the liquid is “linked” to the paste, so that this is the paste which is expected to move and/or dry. If it moves this is due to capillary effects. Let us first examine whether the paste is able to react to capillary effects at the scale of the pores of the bead pack. This is indeed not obvious: for a simple liquid the resistance to flow is negligible at a very small flow rate so that capillary effects are always able to overcome viscous effects at sufficiently low flow rates; for a paste the resistance to flow remains larger than a finite value whatever the flow rate. The appropriate number for this evaluation is the capillary number (Ca), here expressed as the ratio of the yield stress (τ_c) times a characteristic length scale (a) of the sample to the surface tension (γ) of the material. Indeed, the energy dissipated in a sample volume a^3 undergoing a deformation (at a sufficiently slow rate) ε is on the order of $\tau_c a^3 \varepsilon$, while the surface energy stored is on the order of $\gamma a^2 \varepsilon$. The ratio of these two energies gives $\text{Ca} = \tau_c a / \gamma$. Here, a is significantly smaller than the bead diameter (typically 300×10^{-6} m) and $\tau_c = 50$ Pa, so that $\text{Ca} \ll 1$ (using the surface tension of water, as it is the interstitial liquid of the paste). This means that capillary effects at the scale of the pores of the bead pack *a priori* dominate the viscous effects and thus might tend to drive the paste through the porous medium.

Finally in this situation we can again distinguish two asymptotic cases:

(i) Case (c): motion of the paste through the granular packing as a result of capillary forces and drying at the sample surface; in that case the drying rate will be imposed by the external conditions as in case (a) and should have the form given by equation (1); however, as the paste advances toward the free surface and dries the paste elements tend to accumulate and form a crust around the free surface, which might then tend to decrease the drying rate.

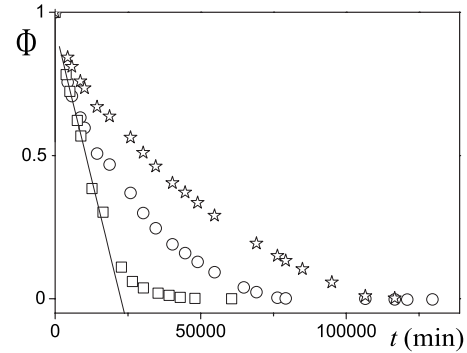


FIG. 4. Drying curves of analogous samples (height: 57 mm; average bead diameter: 300 μm) with different interstitial pastes: kaolin suspension (squares); bentonite suspension (circles); and gel (stars).

(ii) Case (d): the paste remains globally fixed within the porous structure; thus, drying occurs as a result of the advance of a dry front through the granular packing; this case is finally similar to case (b) and the drying rate should have the form of Eq. (2).

In order to determine to which case we are the closest it is thus necessary to have macroscopic information (drying rate) and microscopic information concerning both the distribution in time of water and paste elements.

IV. RESULTS AND DISCUSSION

A. Macroscopic observations

We start by comparing the timing of drying of three samples of identical height but with three different interstitial pastes. Although the porosity of the bead packing was the same for the three samples the initial water mass was different because the solid fraction of each paste was different. However, the maximum difference (between the kaolin sample and the two others) was 15%. We follow the drying curve, i.e., the total saturation versus time. In a linear scale (see Fig. 4) we see that the drying rate ($-d\Phi/dt$) significantly differs for the different materials. It is approximately constant over a wide range of saturations for the kaolin sample but continuously decreases in time for the bentonite and the gel samples. In a logarithmic diagram (see Fig. 5) the curves have a similar shape but they differ by what one can distinguish as a *characteristic time of drying*: the abscissa position of the vertical asymptote. It appears that the characteristic times of drying of the three materials are quite different: it varies by a factor 3 from the kaolin to the gel despite similar overall drying conditions.

This suggests that this is the interstitial paste which plays a fundamental role on the drying characteristics. In order to confirm we carried out tests with beads of different diameters (see the inset of Fig. 5) and even with samples made of two layers (below and above a critical height) with the same interstitial paste but two different bead sizes (see Fig. 5). We conclude that the macroscopic drying characteristics are not affected by the bead diameter in this range. The same conclusion was reached for the bentonite samples.

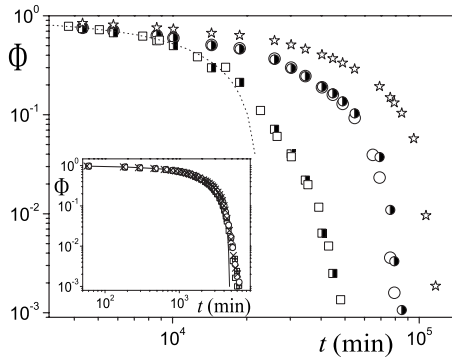


FIG. 5. Drying curves of analogous samples (height: 57 mm) with either one-particle size ($300 \pm 50 \mu\text{m}$) with different interstitial pastes—kaolin suspension (squares), bentonite suspension (circles), and gel (stars)—or with half the packing height (bottom) made of large particles (1 mm) and the other part (top) made of smaller particles ($300 \pm 50 \mu\text{m}$)—kaolin suspension (two-colored squares) and bentonite suspension (two-colored circles). The dotted line is the linear model fitted to kaolin data in Fig. 2. The inset compares the drying curves of different granular packings (with a constant volume fraction of beads: 62%) with a height of 1.5 cm: pure water+beads (continuous line); kaolin paste (25%)+small beads ($300 \pm 50 \mu\text{m}$) (squares); kaolin paste (25%)+intermediate beads ($600 \pm 50 \mu\text{m}$) (circles); kaolin paste (25%)+large beads (1 mm) (crosses); and more concentrated kaolin paste (31%)+small beads ($300 \pm 50 \mu\text{m}$) (cross squares).

Also we can wonder whether these results depend on the rheological behavior of the paste. The results obtained with the kaolin paste at two different solid fractions are exactly the same, although their yield stresses are significantly different. This means that there is no significant impact of the viscous properties of the paste, but obviously this result is true only within some limited range of behavior (and thus of solid fractions) and further study is needed to fully explore this point.

B. Further analysis

1. Kaolin samples

In order to measure the solid fraction of clay remaining at the end of the tests at different levels in the samples we cut some of them perpendicularly to their axis in several portions. Then, we diluted the clay+beads in a large amount of water and cleaned the beads with the liquid so that we were able to separate the beads from a water-clay suspension. Finally, we dried then weighted each material to get the amounts of clay and beads in each portion. Note that the measured relative concentration of bead/clay for the bentonite sample is 45.1 which is very close to the theoretical value according to our sample characteristics: bead volume fraction/clay fraction within the pores [$64\% / (36\% \times 4\%) = 44.4$]. For the kaolin suspension there is a significant discrepancy: the average value is 6.4 whereas the theoretical value is $64\% / (36\% \times 21\%) = 8.5$. We can suspect some uncertainty on the effective fraction of beads in the final mixture. Indeed, after mixing the different materials at the fixed solid fractions we cannot be sure that the bead fraction of the

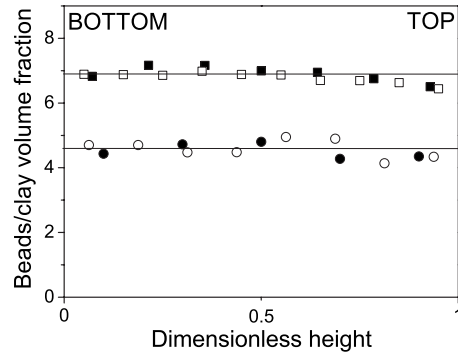


FIG. 6. Bead to clay volume fraction as a function of the height within kaolin (squares) and bentonite samples (circles) (times ten in that case) of two different heights: 69 mm (filled symbols) and 89 mm (open symbols).

mixture effectively put inside the container is exactly 64%; there might be some dilation of the granular packing. If the effective bead fraction is 62% we get a bead/clay fraction of 7.7. This effect nevertheless seems unable to fully explain the discrepancy but we do not have other idea about the origin of this discrepancy.

The essential result of these measurements is that at our scale of observation (typically 0.5 cm) and within the uncertainty on measurements the solid fraction is uniform (see Fig. 6). This means that the solid matrix of the paste remains essentially fixed within the bead pack and the liquid moves through it until reaching a free surface where it can evaporate. This implies that case (c) does not occur.

For the kaolin sample there is a long constant drying rate period which suggests that the first scaling [Eq. (1)] would apply. Indeed, this scaling works very well: the saturation decreases proportionally to the time and all the curves fall along a master curve when the time is scaled by the sample height (see Fig. 7). This observation is in favor of a simple description of the drying of such samples as a process in which the water is drained by capillarity through the solid matrix of the paste (being itself within the granular packing) up to the free surface of the sample. During this process the kaolin paste locally shrinks and air penetrates from the free

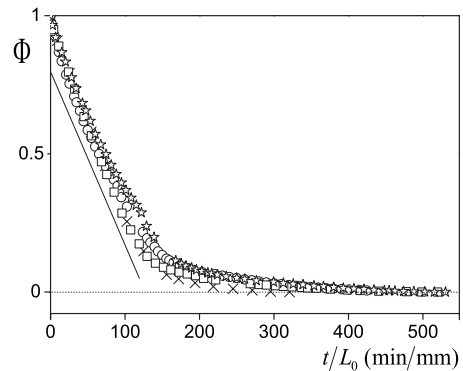


FIG. 7. Drying curves for kaolin samples of different heights as a function of the time scaled by the sample height: 20 mm (crosses), 67 mm (squares), 89 mm (stars), and 145 mm (circles). The straight line is a guide for the eyes.

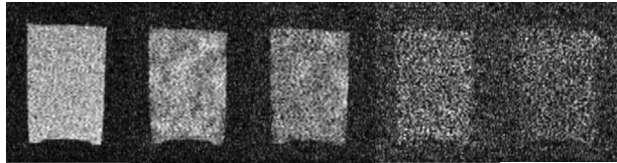
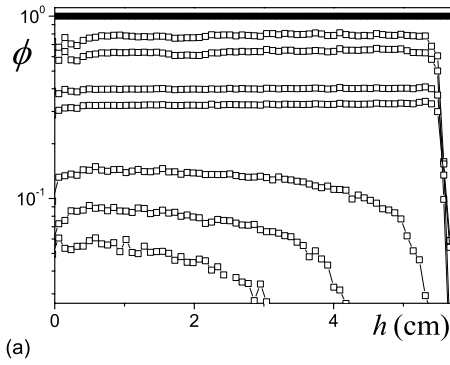


FIG. 8. Density profiles as measured by NMR and then corrected (see text) for a kaolin sample (sample height: 57 mm) at different times during drying: (from top to bottom) 0 (filled squares), 2.5, 5, 8.5, 11, 15, 18, and 20 days. MRI pictures (b) of a longitudinal cross section (see text) along the central axis of the same sample at different times: 0, 2.5, 5, 8.5, and 11 days (sample diameter=white or gray area of 34 mm diameter).

surface to fill the voids thus created. It is noticeable that the scaling by L_0 still works for low saturations when the drying rate is no longer constant but we have no explanation for that.

As suggested by the drying curves we effectively observe from the NMR data [see Fig. 8(a)] a homogeneous saturation down to low values. After some time a dry front starts to progress through the sample from the top while the plateau level inside the sample also decreases. A confirmation of these trends appears from a similar test with a thinner sample (17 mm) which dried sufficiently rapidly so that density profiles could be obtained at shorter intervals until complete drying (by keeping the sample inside the magnet). The results show that the density profiles remain almost perfectly horizontal down to a saturation of about 15%, then a dry front starts to progress in the sample (see Fig. 9). This critical saturation is almost exactly that for which the drying curve starts to significantly depart from a straight line (i.e., constant drying rate) (see Fig. 5). Note that during this stage the top layer of the material seems to slowly dry. This is likely explained by a global shrinkage of the granular paste, as a result of strong capillary forces within the drying paste, and not by a faster drying of the paste around the free surface of the sample. This was confirmed by observation of the sample at the end of the test: the free surface of the sample has been slightly moved down.

These trends result from measurements corresponding to average densities within horizontal layers of materials which might, in fact, be the result of some strong radial heterogeneity of the water density within the sample (such as specific fracture paths through which the water would be drained). We could check that this was not the case from 2D images:

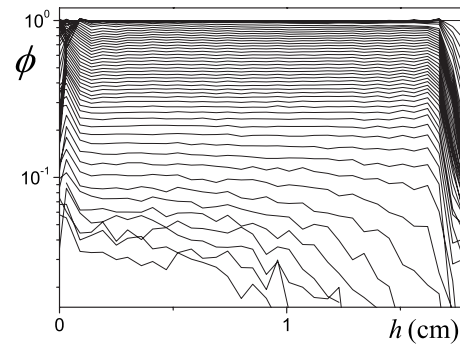


FIG. 9. Water saturation profiles in time as measured by NMR for a kaolin sample with thickness of 17 mm (increasing time from top to bottom). The first seven profiles were measured every 42 min after the beginning of the test; the others were measured for each 120 min.

in these images the local fluctuations cannot be interpreted as effective local variations of the density; they are mainly due to the noise associated with the technique. Moreover, because of relaxation effects the mean signal intensity obtained from such images cannot be directly related to the effective density, so that they simply provide a qualitative appreciation of the relative values of the water saturation, some information of which is sufficient in this context. Under these conditions we see that the mean signal intensity decreases almost homogeneously in the sample in time [see Fig. 8(b)]. Moreover we observe the slight decrease of the top surface in time described above as a result of a possible slight shrinkage of the sample or a drying of the top layers. This confirms each point of a saturation profile corresponds to the average value of the saturation in a cross-sectional layer in which the saturation is everywhere close to this value.

We can now suggest a scheme explaining the different trends observed. First of all it is worth emphasizing that since the water saturation decreases within the kaolin paste while the paste elements do not significantly move through the porous structure there must correspondingly be air entrance within the bead packing in order to fill the voids. Air bubbles progressively invade the sample during this stage. This process is very similar to that observed for pure water within simple bead packing (see [16]). As a consequence it is likely that during this phase capillary forces are the driving forces leading to the re-equilibration of the fluid distribution within the paste. These capillary effects are similar to those which would act on water alone. Here, the only change is that the decrease of liquid amount in the paste leads the paste elements to be progressively displaced and rotated to a more compact configuration within the liquid.

The beginning of the second stage, associated with the critical saturation identified above, likely corresponds to the situation for which open fractures start to develop in the paste. A similar effect is observed with pure kaolin-water pastes: the CRP finishes when fractures start to develop. This is so probably because for a too high clay fraction shrinkage is no longer possible: the clay platelet particles are strongly jammed so that any of them cannot reach more compact position without a rearrangement of the structure around it, which cannot occur spontaneously; extracting more water

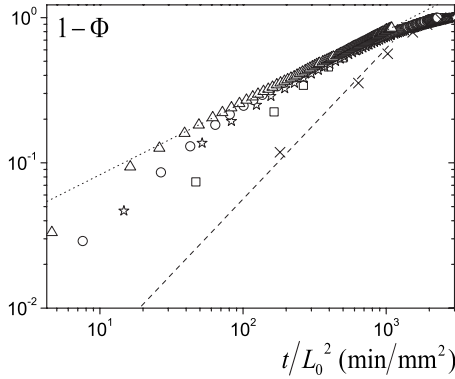
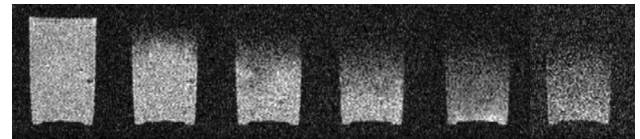
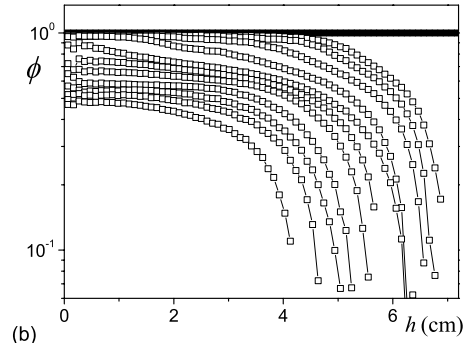
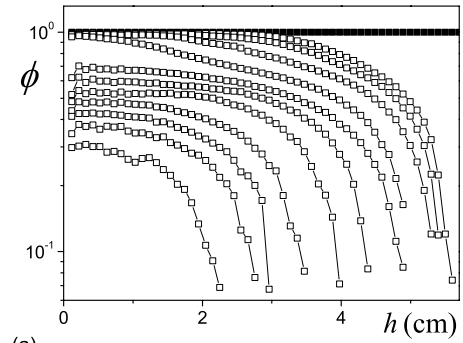


FIG. 10. Drying curves for bentonite samples of different heights as a function of the time scaled by the square sample height: 15 mm (crosses), 34 mm (squares), 67 mm (stars), 89 mm (circles), and 145 mm (triangles).

requires breaking the structure, which induces fractures. These fractures can separate the paste in isolated parts so that the hydraulic continuity with the rest of the sample may be broken. This process does not lead to a homogeneous decrease of the water saturation because its largest influence is basically localized at the dry front, then the fracture propagation leads to a hole within the material generally smaller for larger distances from the fracture opening. Typically, the shape of the air opening resulting from a fracture developed in a pure clay suspension is that of a dihedral which, if we assume that the water fraction within the paste remains homogeneous, should lead to a heterogeneous distribution of the apparent density of water within the sample. Then, it is likely that after some distance the fracture thickness reaches some constant value, which could explain the apparent plateau at some distance from the front (see Figs. 7 and 8). Another possibility is that the fractures tend to create isolated paste islands close to the evaporation front which first completely dry before the dry front further progresses downward. This complex process might explain why we do not observe a drying rate scaling with the square root of the time in the second regime: this is not a simple dry front which progresses in the material while the rest of the material keeps a constant water saturation.

2. Bentonite samples

For the bentonite suspensions the solid fraction of clay remaining after complete drying is also homogeneous (see Fig. 5), which indicates that there is no motion of the paste through the sample. Nevertheless, the results for the other drying characteristics are quite different. The drying curve initially seems similar to that observed for the kaolin (see Fig. 4) but soon its slope significantly decreases. In order to appreciate the impact of the sample size we carried out tests with samples of different heights. The results are presented in Fig. 10 in terms of $(1 - \Phi)$ as a function of time scaled by the square sample height. It appears that the saturation decreases linearly with the time only until such a time that decreases with the sample height. Beyond this time it decreases with the square root of the time and the curves fall along a master curve, as predicted in Eq. (2). This process



(c)

FIG. 11. Density profiles as measured by NMR for bentonite samples [(a) $L_0=57$ mm and (b) $L_0=72$ mm] at different times during drying: (from top to bottom) 0 (filled squares), 3, 4, 6, 10, 18, 21, 24, 28, 31, 34, and 38 days (empty squares). MRI pictures (c) of a longitudinal cross section (see text) along the central axis of sample (b) at different times: 0, 3, 6, 10, 18, and 21 days (sample diameter=white or gray area of 34 mm diameter).

suggests that there is a dry front progressing inward during this period.

Let us now look at the NMR density profiles for the bentonite samples [see Figs. 11(a) and 11(b)]: as soon as drying has started they do not exhibit any plateau, instead the density profile is bent over at the approach of the sample top so that there is both an inward progression of the dry front and a decrease of the water saturation in all the sample situated below this front. Once again from 2D imaging [see Fig. 11(c)] we could check that these measures effectively reflect homogeneous effects in each horizontal layer and not three-dimensional heterogeneities (such as the opening of localized wide air paths through the sample): the mean signal intensity is graduated shading, indicating that the water saturation is larger close to the bottom, and the dry front progresses downward.

The specific shape of these profiles might be explained by the penetration of fractures inside the sample. As for kaolin one can expect that these fractures induce the formation of openings with a dihedral shape, leading to an apparent water saturation decreasing toward the free surface. As drying goes

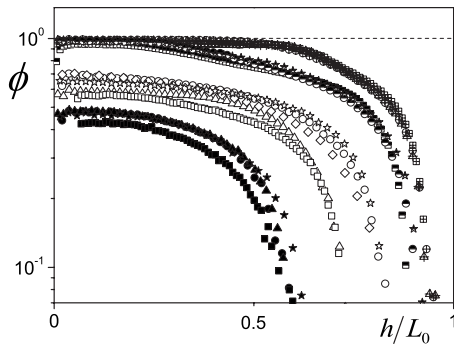


FIG. 12. Water saturation profiles within bentonite samples of different heights (the distance from bottom has been scaled by the sample height) at different times scaled by the square height (successively cross, two-colored, empty, and filled symbols): 11.5 cm (squares) at 109, 261, 806, and 1100 min cm⁻²; 7.2 cm (triangles) at 111, -, 778, and 1056 min cm⁻²; 5.9 cm (circles) at 124, 248, 745, and 1158 min cm⁻²; 4.7 cm (stars) at -, 261, 847, and 1369 min cm⁻²; and 3.4 cm (losanges) at -, -, 747, and - min cm⁻².

on the fractures penetrate farther while the material close to the sample top becomes completely dry. When they reach the sample bottom a new phase starts, leading to a simultaneous decrease of the overall level of the profile and an advance of the dry front downward. As for the kaolin sample the fractures might create islands of paste around the dry front, which will then completely dry. However, the exact processes at work during this phase remain difficult to identify.

Surprisingly, although during this phase there is simultaneously a decrease of the density plateau and an advance of the dry front, the drying rate is well described by a model assuming a simple progression of a dry front. Indeed, $1 - \Phi$ decreases with the square root of the time and a master curve is obtained when scaling the time by the square sample height (see Fig. 10). We have no obvious explanation of that effect. However, we checked the full agreement of this description with our data also at a mesoscopic scale. Indeed, if there is also at this scale a full similarity of the process by scaling the time by the square sample height we should obtain a similarity of the density profiles at different times scaled in a similar way. This is effectively what we get: the density profiles (scaled by the sample height) obtained at similar reduced times are similar at short times of drying and are close to each other at longer times of drying (see Fig. 12) when the effect of uncertainty on the experimental conditions may become stronger.

As we already suggested from our above macroscopic observations these physical processes at work during the drying of such samples are essentially due to the behavior of the interstitial paste as confirmed by the fact that the density profiles are similar for a bilayer sample. There is no significant impact of the bead size: the profiles look similar to those obtained for a uniform sample (see Fig. 13).

3. Gel sample

For the gel the drying rate always decreases (see Fig. 4). Actually, when plotting $1 - \Phi$ as a function of the time we see (see Fig. 14) that it decreases approximately with the

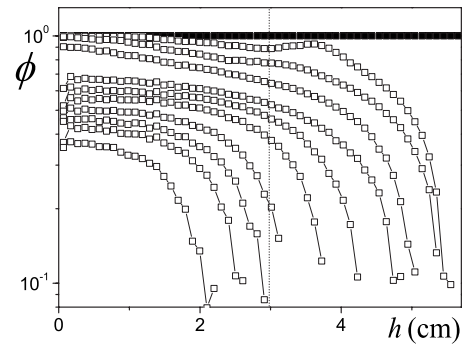


FIG. 13. Density profiles as measured by NMR for a two-layered (diameter: 300 μm above, 1 mm below) bentonite sample ($L_0=57$ mm) at different times during drying: (from top to bottom) 0 (filled squares), 3, 6, 10, 18, 21, 24, 28, 31, 34, and 38 days (empty squares).

square root of the time. Thus, the apparent drying rate could approximately be associated with an inward progression of a dry front. This is consistent with our NMR observations. Indeed, the water saturation profiles are made of two parts [see Fig. 15(a)]: close to the bottom the water saturation remains almost constant while there is clearly a dry front progressing from the sample top. Note however that this front is almost straight at the beginning of the process but progressively bends as it advances downward. From the 2D images we essentially see the progression of a dry front while the water saturation remains almost constant within the rest of the sample [see Fig. 15(b)]. This proves that the trends observed in the water saturation profiles well describe evolutions which are homogeneous in cross sections within the sample.

With the gel we could not get accurate data for the final distribution of the solid fraction of the gel in the sample after complete drying. However, the aspect of the profiles of water saturation implies that there is no upward motion of the gel: the top layers successively dry at their initial position.

C. Synthesis

After this detailed description of the drying characteristics we are now able to explain the initial observation about the

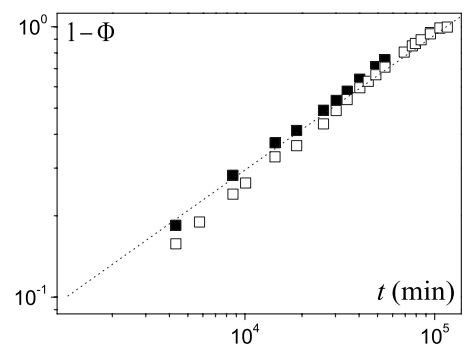
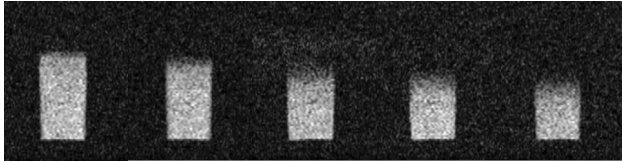
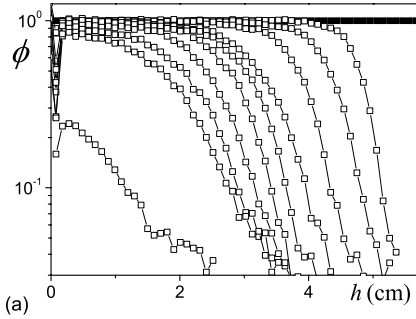


FIG. 14. Drying curve for the gel sample in terms of the evaporated water fraction: deduced from sample mass measurements (open squares) or computed from MRI profiles without signal correction (filled squares). The dotted line has a slope of $\frac{1}{2}$.



(b)

FIG. 15. Density profiles as measured by NMR for the gel samples at different times during drying: (from top to bottom) 0 (filled squares), 3, 6, 10, 18, 21, 24, 28, 31, 34, 38, and 66 days. MRI pictures (b) of a longitudinal cross section (see text) along the central axis of the same sample at different times: 3, 6, 13, 18, and 21 days (sample diameter=white or gray area of 34 mm diameter).

characteristic drying times, i.e., the fact that drying the different paste-grain samples under similar external conditions and with similar amount of water inside leads to very different characteristic times of drying. Actually, we have a clear qualitative explanation: for the kaolin suspension the drying relies on a capillary transport toward the sample surface, while for the gel it mainly relies on the diffusion of vapor from the dry front toward the sample surface; the first process leads to a much more rapid evaporation than the second one, in consistence with usual explanations for the CRP and the FRP. For example, with simpler systems (bead packing + water) similar significant differences in characteristic drying times were observed depending on the drying process (capillary transport or vapor diffusion) [16]. In this context the drying characteristics of the bentonite sample are intermediate, as it involves both dry front withdrawing and capillary transport from the bottom layers. However, we can hardly go further and propose a straightforward quantitative prediction of the effective saturation variations in time in each case. Indeed, there are several aspects that can affect the exact rate of evaporation and that we cannot *a priori* quantify properly such as the diffusion coefficient through the porous matrix, the shape of the paste-air interface along the sample surface, the detailed shape of the dry front inside the material, etc.

Now the question is why pasty materials of similar overall aspects and, in particular, similar rheological characteristics can yield significantly different drying processes. The explanation likely lies in their specific internal structures, which are completely different (see Sec. II A). As a consequence the forces vary quite differently as a function of the distance between the elements. This implies that the impact of water withdrawing (which reduces the average distance) on the structure characteristics can significantly vary from one ma-

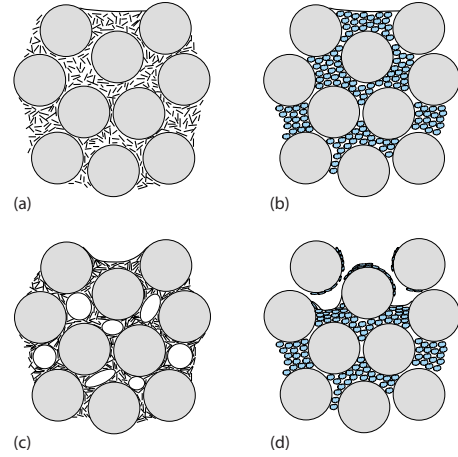


FIG. 16. (Color online) Schemes of drying processes of pastes in bead packing. (a) Kaolin suspension and (b) Carbol gel saturating bead packing evolve in two different ways. For the kaolin air penetrates by capillary effects inside the porous medium; (c) the solid kaolin particles get closer to each other and the paste concentration increases homogeneously throughout the sample. (d) For the gel only the elements close to the free surface are squeezed and finally dried, air penetrates in the form of a front progressing through the sample.

terial to the other. For kaolin suspensions the colloidal forces between elements are very weak so that capillary forces throughout the liquid network can induce a homogeneous shrinkage of the paste inside the granular packing. This leads to the scheme of Fig. 16(a), which differs from that for pure water in a granular packing only by the fact that the remaining liquid becomes more viscous as drying progresses. For the gel, extracting water implies to shrink each element of the paste, which requires a significant energy. This might explain that the evaporation along the gel-air interface is able to shrink the elements close to this interface but capillary forces are unable to shrink the elements inside the porous system far from the air-gel interface. This corresponds to the scheme of Fig. 16(b). For the bentonite paste we now have strong attractive forces which might induce shrinkage along with fractures, leading to a complex process with drying characteristics intermediate between the gel and the kaolin. However, more insight in the processes is required to really understand that case.

V. CONCLUSION

Our results show that the drying of granular pastes, made of a fine paste embedded in a granular packing, is mainly governed by the paste structure. When the elements suspended in the paste can be approached easily the drying characteristics are very close to those observed for pure water inside a granular packing. In particular, there exists a long initial CRP governed by capillary effects. When large forces are necessary for approaching the paste elements to each other capillary effects are no longer dominant and more complex effects such as fractures throughout the material may occur. A partial or full dry front may develop, leading to a much slower drying rate of the granular packing.

This suggests that it is possible to act on the drying rate of soils by modifying the interstitial paste around the surface of the material: for example, if one is able to inject a gel in the top layers of the soil, a dry front will form soon, significantly slowing down the drying rate of the whole soil which otherwise would have dried during a long period, thanks to capillary effects draining water to the free surface of the sample. This also suggests the possibility of devising civil engineering pasty materials with specific drying properties associated with specific evolution of the water distribution in time within the porous structure. Another possible interest of this approach is that it suggests a way for studying the structure of pastes since here we have been able to relate qualitatively the drying characteristics of pastes with the interactions between the elements. In this context an original property of these experiments is that the granular packing let the paste dry under more or less “fixed” boundary conditions, i.e., within a given porous structure and with fixed vapor density

along the free surface of the sample. This contrasts with the drying of pastes alone during which the free surface of the paste in contact with ambient air significantly changes as a result of shrinkage and fractures.

However, our study also shows the need for sophisticated techniques for understanding the origin of specific drying properties of complex materials such as soils or more generally granular pastes. Here, MRI made it possible to get a clear view of the processes at work during the first stage of drying with the kaolin and the gel samples. This technique also provided critical information about the next stages of drying for the different materials. Nevertheless, this information is still incomplete and in order to get a complete understanding of the phenomena in those cases it seems necessary to use other techniques (such as confocal microscopy) to get visualization at a more local scale (that of the grains) within the porous structure.

-
- [1] S. Devahastin, *Mujumdar's Practical Guide to Industrial Drying* (Exergex, Montreal, 2000).
- [2] W. Jury, W. R. Gardner, and W. H. Gardner, *Soil Physics* (Wiley, New York, 1991).
- [3] A. A. Suleiman and J. T. Ritchie, *Soil Sci. Soc. Am. J.* **67**, 377 (2003).
- [4] S. B. Idso, R. J. Reginato, R. D. Jackson, B. A. Kimball, and F. S. Nakayama, *Soil Sci. Soc. Am. Proc.* **38**, 831 (1974).
- [5] D. R. Weinberger, *J. Struct. Geol.* **21**, 379 (1999); H. Peron, T. Hueckel, L. Laloui, and L. B. Hu, *Can. Geotech. J.* **46**, 1177 (2009).
- [6] A. Rose, *Eur. J. Soil. Sci.* **47**, 21 (1996).
- [7] A. A. Van de Griend and M. Owe, *Water Resour. Res.* **30**, 181 (1994).
- [8] J. T. Ritchie, *Water Resour. Res.* **8**, 1204 (1972).
- [9] J. Van Brakel, in *Advances in Drying*, edited by A. S. Mujumdar (Hemisphere, Washington, D.C., 1980), Vol. 1, p. 217.
- [10] P. Coussot, *Eur. Phys. J. B* **15**, 557 (2000).
- [11] P. Lehmann, S. Assouline, and D. Or, *Phys. Rev. E* **77**, 056309 (2008).
- [12] N. Shokri, P. Lehmann, and D. Or, *Geophys. Res. Lett.* **35**, L19407 (2008).
- [13] N. Shokri, P. Lehmann, P. Vontobel, and D. Or, *Water Resour. Res.* **44**, W06418 (2008); P. Lehmann and D. Or, *Phys. Rev. E* **80**, 046318 (2009).
- [14] P. Coussot, C. Gauthier, D. Nadji, J. C. Borgotti, P. Vié, and F. Bertrand, *C.R. Acad. Sci., Paris* **327**, 1101 (1999).
- [15] N. Shokri, P. Lehmann, and D. Or, *Water Resour. Res.* **45**, W02415 (2009).
- [16] N. Shahidzadeh-Bonn, A. Azouni, and P. Coussot, *J. Phys.: Condens. Matter* **19**, 112101 (2007).
- [17] L. Xu, S. Davies, A. B. Schofield, and D. A. Weitz, *Phys. Rev. Lett.* **101**, 094502 (2008).
- [18] A. G. Yiotis, A. G. Boudouvis, A. K. Stubos, I. N. Tsimpanogiannis, and Y. C. Yortsos, *Phys. Rev. E* **68**, 037303 (2003).
- [19] F. Chauvet, P. Duru, S. Geoffroy, and M. Prat, *Phys. Rev. Lett.* **103**, 124502 (2009).
- [20] I. N. Tsimpanogiannis, Y. C. Yortsos, S. Poulou, N. Kanellopoulos, and A. K. Stubos, *Phys. Rev. E* **59**, 4353 (1999).
- [21] J. B. Laurindo and M. Prat, *Chem. Eng. Sci.* **53**, 2257 (1998).
- [22] A. G. Yiotis, A. G. Boudouvis, A. K. Stubos, I. N. Tsimpanogiannis, and Y. C. Yortsos, *AIChE J.* **50**, 2721 (2004).
- [23] P. Coussot, *Rheometry of Pastes, Suspensions and Granular Pastes* (Wiley, New York, 2005).
- [24] J. O. Carnali and M. S. Naser, *Colloid Polym. Sci.* **270**, 183 (1992).
- [25] J. M. Piau, *J. Non-Newtonian Fluid Mech.* **144**, 1 (2007).
- [26] P. Coussot, *Phys. Rev. Lett.* **74**, 3971 (1995).
- [27] P. Coussot, H. Tabuteau, X. Chateau, L. Tocquer, and G. Ovarlez, *J. Rheol.* **50**, 975 (2006).
- [28] N. Roussel, R. Le Roy, and P. Coussot, *J. Non-Newtonian Fluid Mech.* **117**, 85 (2004).
- [29] H. H. Macey, *Trans. Brit. Ceram. Soc.* **41**, 73 (1942).
- [30] G. W. Scherer, *Cem. Concr. Res.* **29**, 1149 (1999); *J. Am. Ceram. Soc.* **73**, 3 (1990).
- [31] S. Philippot, J. P. Korb, D. Petit, and H. Zanni, *Magn. Reson. Imaging* **16**, 515 (1998).
- [32] H. Y. Carr and E. M. Purcell, *Phys. Rev.* **94**, 630 (1954); S. Meiboom and D. Gill, *Rev. Sci. Instrum.* **29**, 688 (1958).